ACS APPLIED MATERIALS & INTERFACES

Research Article

www.acsami.org

In Situ Preparation of 1D Co@C Composite Nanorods as Negative Materials for Alkaline Secondary Batteries

Cuihua An, Yijing Wang,* Yanan Xu, Ying Wang, Yanan Huang, Lifang Jiao, and Huatang Yuan

Institute of New Energy Material Chemistry, Collaborative Innovation Center of Chemical Science and Engineering (Tianjin), Key Laboratory of Advanced Energy Materials Chemistry (MOE), Tianjin Key Lab of Metal and Molecule-based Material Chemistry, Nankai University, Tianjin 300071, People's Republic of China

Supporting Information

ABSTRACT: Cobalt-based coordination compounds were successfully prepared via employing nitrilotriacetic acid (NTA) as a complexing agent through a mild surfactant-free solvothermal process. Cobalt ions are linked with the amino group or carboxyl groups of NTA to become one-dimensional nanorods that can be proved by Fourier transform infrared measurement findings. The morphologies of the precursor Co−NTA highly depend on the solvent composition, the reaction time and temperature. The probable growth mechanism has been proposed. After heat treatment, the Co−NTA precursor can be completely converted into Co@C nanorods assembled by numerous core−shell-like Co@C nanoparticles, which preserved the rodlike morphology. The as-prepared Co@C composites display a rodlike morphology with 4 μm length and 100 nm diameter. The electrochemical performances of this novel Co@C material as the alkaline secondary Ni/Co battery negative electrode have been systematically researched. The discharge capacity of the Co@C-1 composite electrode can attain 609 mAh g^{-1} and retains about 383.3 mAh g^{-1} after 120 cycles (the discharge current density of 500 mA g^{-1}). The novel material exhibits a high discharge capacity of 610 and 470 mAh g^{-1} at discharge currents of 100 and 1000 mA g^{-1}, respectively. This suggests that approximately 77% of the discharge capacity is kept when the discharge current density is increased to 1000 mA g^{-1} (10 times the initial current density of 100 mA g^{-1}). The excellent electrochemical properties could be ascribed to the porous channels of the novel Co@C materials, which is beneficial to electrolyte diffusion and electrons and ions transportation.

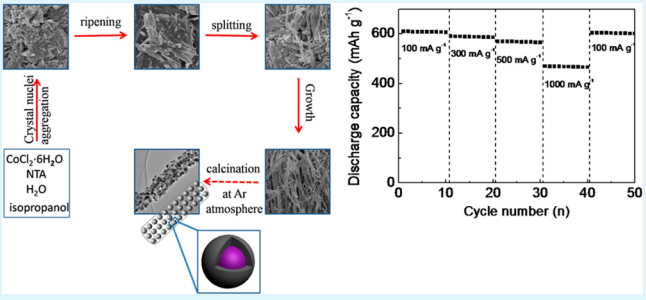

KEYWORDS: *In situ, solvothermal, Co@C nanorod, core−shell-like nanoparticles, alkaline secondary battery*

1. INTRODUCTION

It is well-known that not only the composition but also the phase, morphologies, size and size distribution have an important impact on the inherent characters of the inorganic materials.[1−3] Therefore, preparation of inorganic materials with particular compositions has been meaningful for developing functional materials and much effort has been undertaken.[4−7] Synthesis of one-dimensional (1D) structures, for example, rods, wires, tubes and belts, have been extensively studied for energy storage.[8−12] The unique functional properties of such structures, including high specific area and large channels among the nanostructures, provide many reaction sites for facile charge transfer and electrolyte penetration. 1D nanostructures may further boost the electrical conductivity and contribute the redox reaction because of the rapid ion and electron transportation process. Thus, for modifying their chemical and physical properties, many attempts have been devoted to prepare 1D nanomaterials, and thus improve their properties especially as the anode for alkaline rechargeable Ni/Co batteries, which adopted $Ni(OH)_2$ as the positive materials and Co-based materials as the negative materials in an alkaline aqueous solution.[13−16]

Alkaline rechargeable batteries, the most promising energy-storage equipment with a high energy and power density and low price, have attracted considerable attention because of their wide applications in many aspects.[17,18] An increased focus has been put on Ni/Co batteries as a new electrochemical energy storage solution for alkaline rechargeable batteries. In this battery system, $Ni(OH)_2$ is employed as the cathode and $Co(OH)_2$ as the anode. According to Gao et al.,[13] this battery type has a specific energy of about 160 Wh kg^{-1}, which is much higher than the 70−90 Wh kg^{-1} of commercial Ni/MH batteries. Compared to cathode materials, recent research pays more attention to the anode materials. Recently, more and more research has focused on Co-based materials that include cobalt oxides and hydroxides, Co-based alloys as the anode of the rechargeable Ni/Co batteries.[15,19−22] The above-discussed electrodes present a higher discharge capacity, more excellent cycle performances and rate capability than other materials. And the active substance to react during the charge/discharge

Received: October 31, 2013
Accepted: February 26, 2014
Published: February 26, 2014

procedure was demonstrated to be metallic Co. Therefore, the discharge capacity of Co-based negative materials could be mainly attributed to the utilization of Co. Co−carbon materials, for instance, Co−carbon nanotubes (CNTs) (prepared via hydrothermal method), Co−CNTs (obtained by ball-milled) and Co/CMK (synthesized by hydrothermal way) have been covered to exhibit good electrochemical properties.[16,23,24] Not only is the active substance dispersion improving but also the materials electroconductibility is undergoing improvement after introducing carbon to the anode.[25,26] Moreover, porous Co@C nanostructures with enhanced surface area, good capability to alleviate large volume changes and more electroactive sites have also been demonstrated to reinforce the electrochemical ability. However, the existing methods to synthesize the Co−carbon composites are distinctly painful and industrially unable with tedious and time-consuming processes.

Therefore, a novel self-template tactic has been verified for the in situ preparation of 1D Co@C composites via a solvothermal method, employing nitrilotriacetic acid (NTA) as the carbon source, and the precursor Co−NTA serves as the built-in template in the following annealing procedure. During the heat treating process, the core−shell-like Co@C nanoparticle structure comes into being due to the fracture of an atomic bond, which leads to the high surface area and porous structure. These Co@C nanoparticles are intercrossed and interconnected with one another, forming an intricate transportation network to provide an excellent capability for fast ions and electron transfer. Because of the low cost of Co−NTA, it would be industrially feasible. Moreover, this method avoids the use of hard templates, complex activations, corrosive chemicals and specific precursors. The obtained 1D Co@C nanorods own an elaborate 1D nanostructure and a three-dimensional (3D) interconnected mesoporous structure, uniform mesopore size (18.1 nm) and high surface area (94.5 m^2 g^{-1}), which give rise to excellent performance as the negative material in an alkaline Ni/Co battery. When evaluated as the negative materials of the alkaline rechargeable battery, they show a high initial discharge capacity (609 mAh g^{-1}) and could retain a high reversible capacity of 383.3 mAh g^{-1} after 120 cycles at a discharge current of 500 mA g^{-1}. These excellent results reveal that such uniquely structured Co@C nanorods are promising in electrochemical energy storage applications.

2. EXPERIMENTAL SECTION

2.1. Synthesis. Cobalt chloride hexahydrate ($CoCl_2{\cdot}6H_2O$) and NTA were purchased from Alfa Aesar China Co., Ltd. The 1D mesoporous Co@C nanorods were synthesized through solvothermal methods followed by an annealing process. In a synthesis procedure of the precursor, 1.5 g of $CoCl_2{\cdot}6H_2O$ and 0.6 g of NTA were added to 10 mL of distilled water with vigorous stirring until dissolution. Then 30 mL of isopropyl alcohol (IPA) was added to the above solution with stirring for another 10 min. The mixed solution was transferred into a 50 mL Teflon-lined autoclave and then put in a drying oven. The temperature was set in 180 °C and maintained for 6 h. The precipitation was gathered by centrifugation, and washed with distilled water and anhydrous ethanol for six times. After that, the collected product was dried at 60 °C overnight in an oven. The obtained product was named H1. The precursors H2 and H3 were prepared in a mixture (20 mL of distilled water and 20 mL of IPA) and 40 mL of IPA, respectively, without other changes. The 1D porous Co@C nanorods were obtained by calcination of the precursor H1, H2 and H3 at 500 °C for 2 h in Ar atmosphere. The corresponding samples prepared from the precursor H1, H2 and H3 were designated as Co@C-1, Co@C-2 and Co@C-3, respectively. The productivity of the 1D Co@C nanorods can be calculated by the following equation:

$$\text{productivity} = \frac{m_{\text{actual}}}{m_{\text{theorotical}}} \times 100\% \quad ([1])$$

in which m_{actual} is the actual mass value of the element Co in the Co@C composite after the thermal reaction, $m_{\text{theoretical}}$ is the theoretical mass value of the element Co in the as-prepared Co@C composite. The actual mass of the Co@C-1, Co@C-2 and Co@C-3 composites are 0.1747, 0.1108, and 0.1282 g, respectively. The cobalt contents of the as-prepared Co@C-1, Co@C-2 and Co@C-3 were characterized by ICP and the amounts of the Co are 68%, 73% and 78%, respectively. So, the element Co mass of the Co@C-1, Co@C-2, Co@C-3 composites are 0.1188, 0.0809, and 0.0999 g, respectively. The theoretical Co mass is 0.3715 g. Therefore, the productivities of the as-synthesized Co@C-1, Co@C-2 and Co@C-3 are 32%, 22% and 27%, respectively.

2.2. Structural Characterization. The composites of the obtained Co@C-1, Co@C-2 and Co@C-3 were determined by powder X-ray diffraction (XRD, Rigaku D/Max-2500). The morphologies were conducted by scanning electron microscopy (SEM, JEOL JSM-6700F field emission), transmission electron microscopy (TEM), high-resolution transmission electron microscopy (HRTEM) and energy-filtering transmission electron microscopy (EFTEM) on a JEOL JEM-2100 transmission electron microscope. The thermal performance of the Co−NTA coordination compound has been investigated by the thermogravimetric analyzer-derivative thermogravimetry technique (TG-DTA, TG209). The obtained Co@C-1 composites were conducted by the X-ray photoelectron spectrometer (XPS, PHI 5000 Versaprobe, ULVAC PHI). Raman spectrum of the Co@C-1 composite was determined by Renishaw inVia (excitation 514.5 nm). FTIR spectra of the precursor H1 and the pure NTA were determined by a FTIR-650 spectrometer (Tianjin Gangdong, resolution of 4 cm^{-1}). Nitrogen adsorption/desorption measurements (NOVA 2200e, Quantachrome Instruments) were performed to characterize the BET specific surface areas and porous instincts of the obtained Co@C composite. And the Co amounts of the Co@C-1, Co@C-2 and Co@C-3 were determined by inductively coupled plasma optical emission spectrometry (ICP-OES, ICP-9000).

2.3. Electrochemical Characterization. The Co@C composite electrode was fabricated through a new smear method. In a typical process, 25% the obtained Co@C composite active material, 70% carbonyl nickel powders and 5% polyvinylidene fluoride were mixed together. After the solution was stirred for about 30 min, the above mixture changed to a paste and then was pressed on a Ni foam (2 × 2 cm) at a pressure of 10 kgf $(cm^2)^{-1}$ for 30 s.

Electrochemical tests of the anode were performed in a three-compartment cell. The Co@C composite electrode was the working electrode. The $NiOOH/Ni(OH)_2$ were the counter electrode. The Hg/HgO served as the reference electrode. A 6 M KOH aqueous solution was the electrolyte.

A LAND battery-test instrument (CT2001A) was used to test the cyclic performances and rate capability of the Co@C composite electrodes. The electrodes were fully charged at 500 mA g^{-1} for 1.5 h, standing for 5 min and then discharged at 500 mA g^{-1} up to −0.5 V (vs Hg/HgO reference electrode). All of the electrochemical measurements were carried out at 25 °C.

3. RESULTS AND DISCUSSION

3.1. Synthesis and Characterization of the Obtained Co@C Nanorod. The morphology of the precursor H1 was determined by SEM and TEM. The SEM images in Figure 1a,b distinctly display that the obtained precursor H1 are made up of nanorods of about 8 μm in length. The representative TEM images (Figure 1c,d) of the obtained precursor H1 show that the precursor H1 has a smooth surface. The average diameter of the precursor H1 nanorod is about 150 nm (Figure 1d). The FTIR spectra in Figure 1e show the composition of the obtained precursor H1 and NTA. According to the literature,[27−29] the band between 3100 and 2900 cm^{-1} is

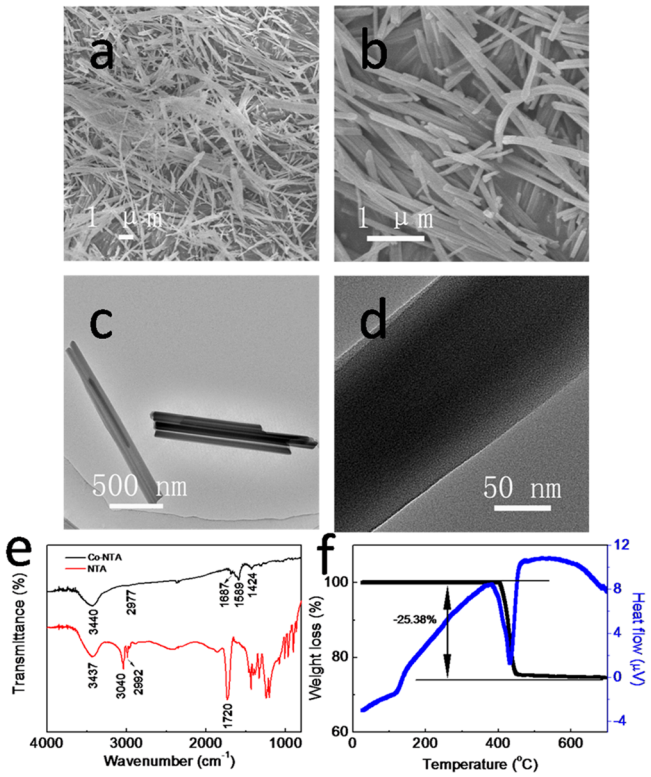

Figure 1. SEM images (a, b) and TEM images (c, d) of the Co−NTA precursor, FTIR spectra (e) of pure NTA and Co−NTA precursor, the thermogravimetric analysis and different thermal analysis (TG-DTA) curve (f) of the Co−NTA precursor.

designated for the stretching vibration of C−H. For precursor H1, due to the introduction of Co^{2+}, the peak at 3040 cm^{-1} disappears, and the peak centered at 2992 cm^{-1} shifted to 2977 cm^{-1}. For NTA, the band located at 1720 cm^{-1} is referred to the stretching vibration of C═O.[9,30,31] But the peak in precursor H1 disappears, and two peaks located at 1687 and 1589 cm^{-1} appear instead, demonstrating the formation of Co−NTA coordination.[32] The TG-DTA technique was employed to research the thermal stability of the precursor H1 (Figure 1f). It is shown that the mass of the precursor H1 changed little when the temperature was below 400 °C. Above 400 °C, the weight loss can be as high as about 25.38%, which is ascribed to the decomposition of the Co−NTA coordination to the Co@C composite. On the basis of the above discussions, to ensure complete decomposition of the Co−NTA precursor, the calcinations temperature of the Co−NTA coordination to the Co@C composite was set at 500 °C for 2 h.

After an annealing treatment at 500 °C, three target products were formed. As shown in Figure 2, the three samples have almost the same XRD pattern, which agrees well with the standard cubic Co phase (JCPDS card no. 89-4307), and the broaden peak around 25° can be ascribed to the amorphous carbon. The diffraction peaks centered at 44.4, 51.7 and 76.0° can be indexed to the (111), (200) and (220) planes of Co, respectively. The unit cell dimension of the structure, a_o, for Co@C-1, Co@C-2 and Co@C-3 is calculated as 3.539, 3.540, 3.538 Å, which is each very close to the value of 3.544 Å given in the JCPDS card no.89-4307 file for Co. In the XRD patterns, except for the peaks of Co and amorphous C, there are no other peaks are observed, indicating the full transformation of the Co−NTA coordination to the Co@C composite. The

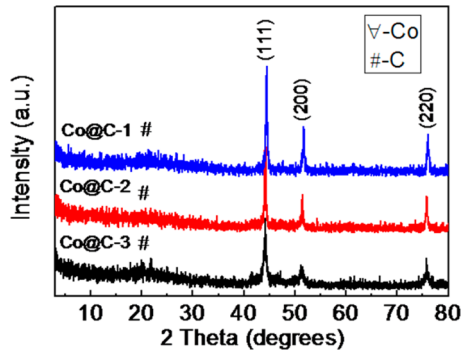

Figure 2. XRD patterns of the as-prepared Co@C-1, Co@C-2 and Co@C-3 composite.

cobalt contents of the obtained Co@C-1, Co@C-2 and Co@C-3 were conducted by ICP and the amounts of the Co are 68%, 73% and 78%, respectively.

SEM and TEM were used to characterize the morphology of Co@C-1 (Figure 3). Co@C-1 displays a rodlike structure with

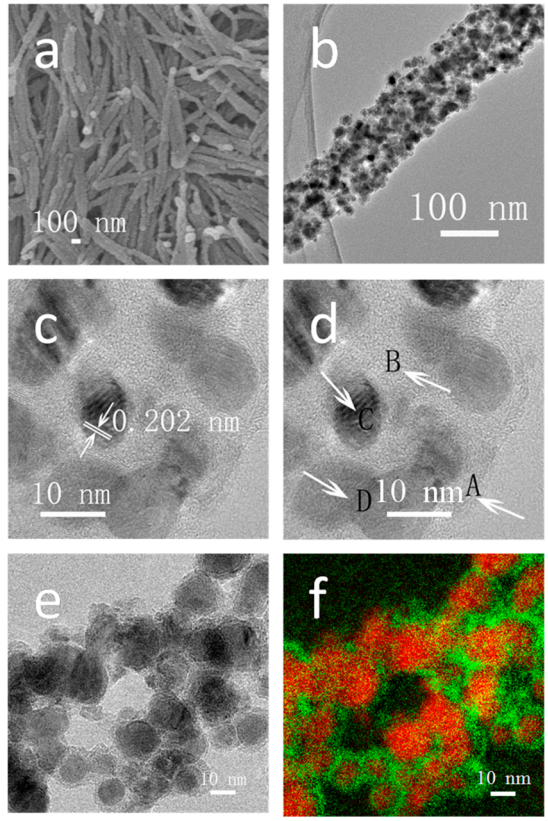

Figure 3. SEM image (a), TEM images (b−d) and EFTEM images (e,f) of the prepared Co@C-1 composite.

about 4 μm length and 100 nm diameter. Thus, the SEM image shows that the Co@C-1 nanorods are made up of a number of nanoparticles, which may be more beneficial to electron transfer. The TEM image shown in Figure 3b further confirm the rodlike structure assembled by Co@C nanoparticles. Figure 3c shows that the fringe spacing is about 0.202 nm, which can be referred to the (111) plane of cubic Co. We can also find that the nanoparticle is composed of Co nanoparticles coated by carbon. As we can see from the HRTEM image in Figure 3d, the amorphous carbon is in the places notes as A and B, while

dx.doi.org/10.1021/am4048392 | ACS Appl. Mater. Interfaces 2014, 6, 3863−3869

the Co nanoparticles (places noted C and D) also exist in the porous Co@C composite. Thus, the synthesized Co@C-1 composite has a Co core of approximately 10 nm in diameter and a carbon shell of about 2 nm in thickness, which are verified by the EFTEM images (Figure 3e,f). Remarkably, the obtained Co@C-1 composite totally retains the 1D structure of the precursor H1, which indicates its thermal stability (Figure 3).

In the XRD patterns (20° to 30°) of the porous Co@C-1 composite, a weak and broad peak from amorphous carbon can be seen clearly (Figure S1a, Supporting Information). The Raman spectrum of the Co@C-1 composite is depicted in Figure S1b (Supporting Information) in which there are two peaks and can belong to the disordered band (D band) (1367 cm^{-1}) and graphene band (G band) (1599 cm^{-1}). The peaks are very broad, which indicates that the carbon structure is amorphous. To further examine the carbon, the graphitization degree I_D/I_G (the intensity ratio of the D band to the G band) is calculated. The I_D/I_G of the prepared Co@C-1 composite is 0.78, which is much higher than that of fully graphitized carbon (0.09).[33−36] This result also proved the carbon is amorphous, which gave a buffer space to volume expansion and improved the conductivity of the composite.

XPS measurement was performed to evaluate the chemical state of the elements in the as-prepared Co@C-1 composite. The Co 2p and C 1s spectra are presented in Figure 4a,b,

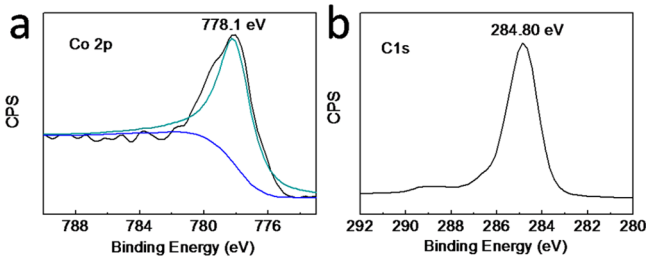

Figure 4. XPS spectra of Co 2p (a) and C 1s (b) for the as-prepared Co@C-1 composite.

respectively. As we can see from Figure 4a, the peak centered at 778.1 eV can be ascribed to the binding energy of Co $2p_{3/2}$, which indicates that the zero valence of Co exists. And the peak located at 284.80 eV (Figure 4b) is well-referred to the sp^2 C-sp^2 C. The above results illustrate that the zero valence of Co and C come into being after calcination.

It is widely accepted that the intrinsic properties of the solvent have impressive effects on the physical and chemical behaviors of the chemicals and the intermediates. Herein, different volume ratios between the distilled water and IPA are employed and the corresponding samples were obtained. It can be seen that both the precursors H2 and H3 display a rodlike structure. Figure S2a,c (Supporting Information) reveals that H2 and H3 are uniform rodlike structures; the product Co@C-2 obtained after annealing H2 displays rodlike structure assembled by a number of nanoparticles, whereas Co@C-3 prepared after annealing H3 is entirely composed of various nanoparticles (Figure S2b,d, Supporting Information). It seems that the distilled water is favorable for the formation of the nanorods structure.

The effect of synthesis condition on the phase formation was investigated via regulating the reaction factors containing the dwell time and the reaction temperature. Figure S3 (Supporting Information) displays SEM images of different precursors prepared at different reaction times. At the initial step, the purple precursor H1 is made up of bulk particles with a little amount of splitting rods on them (Figure S3a,b, Supporting Information). In the following stage, the bulk was splitting the rodlike structures and finally the entire rod shape (Figure S3c,d, Supporting Information). The conditional experiments also show that the precursor H1 possessed different morphologies that can be obtained through varying the solvothermal temperature (Figure S4, Supporting Information).

Scheme 1 displays the probable growth mechanism of the as-prepared composite assembled by numerous core−shell-like

Scheme 1. Schematic Illustration for the Possible Growth Mechanism of the As-Prepared Composite Assembled by Numerous Core−Shell-Like Co@C Nanoparticles

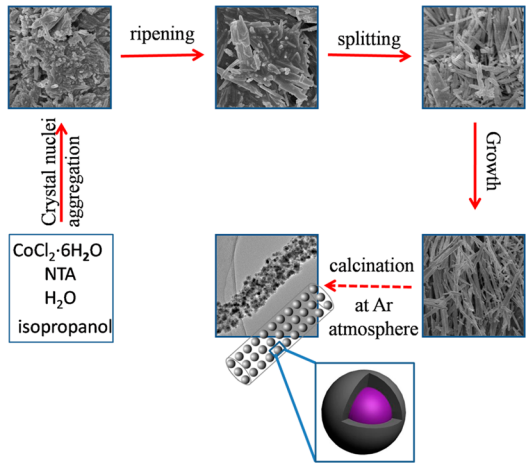

Co@C nanoparticles. At the initial step, metal cobalt ions and NTA molecules become a ternary complex Co−NTA during the solvothermal process. The bulk Co−NTA precursors split to the rodlike structures and finally an entire rod shape with increased dwell time. Then Co@C nanorods preserved the precursor morphology could be synthesized after the thermal treatment of the Co−NTA precursor. During the heat treating process, the core−shell-like Co@C nanoparticle structure comes into being due to the fracture of atomic bond, which leads to the high surface area and porous structure. On the basis of the discussions in the above, the probable growth process of the Co@C-1 composite can be summarized in Scheme 1.

The porosity of the as-prepared Co@C composite is further investigated by BET analysis. The N_2 adsorption/desorption isotherm and the corresponding pore-size distribution plot of the Co@C-1 composite are displayed in Figure 5 and the inset therein. The isotherm can be ascribed as a type IV isotherm, along with H3 hysteresis loops in the 0.5−0.95 relative pressure range, demonstrating the existence of a mesoporous structure. The BET surface area of the Co@C-1 composite is around 94.5 $m^2\ g^{-1}$. Moreover, the pore size distributions indicate that almost pore size is 18.1 nm. The specific surface areas of Co@C-2 and Co@C-3 are about 89.2 and 85.5 $m^2\ g^{-1}$, respectively (Figure S5a,b, Supporting Information). It is well-known that the relatively large surface area and porous features are critical to offer more active sites within pores for fast electrochemical reaction and facilitate the ions and electrons transfer in the electrolyte/electrode interface, resulting in greatly enhanced energy storage performances.

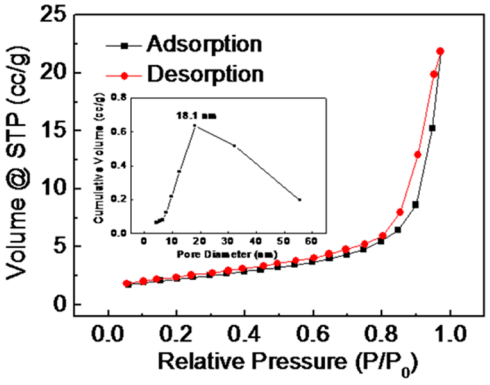

Figure 5. N_2 adsorption/desorption isotherm and the pore size distribution (inset) of the Co@C-1 composite.

3.2. Electrochemical Performances. Owing to the 1D porous structure, core−shell-like Co@C nanoparticles and small particle size, these obtained Co@C samples might be advantageous for electrochemical energy storage. On the basis of the Faraday's law and two-electron reaction during the charge/discharge procedure, the theoretical electrochemical capacities of Co, Co@C-1, Co@C-2 and Co@C-3 are calculated to be 909, 618, 664 and 709 mAh g^{-1}, respectively. Figure 6a displays the cycle performances of the Co@C-1,

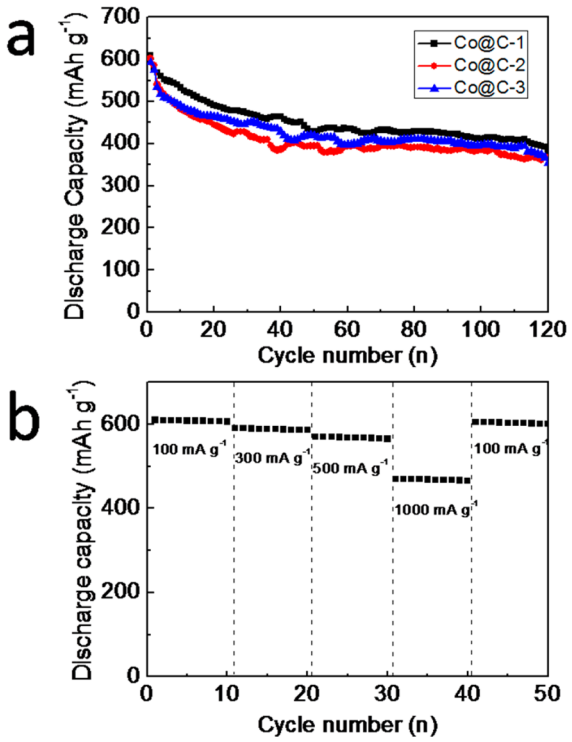

Figure 6. Cycle Curves (a) of the as-prepared Co@C-1, Co@C-2 and Co@C-3 composite electrodes at a current rate of 500 mA g^{-1}, and rate capability (b) of the Co@C-1 composite electrode.

Co@C-2 and Co@C-3 composites as the negative electrode materials of alkaline rechargeable batteries. As it can be seen, the Co@C-1 electrode shows the highest discharge capacity and best cycle performance among the three samples. And the maximum discharge capacity can reach 609 mAh g^{-1}, which is very close to the theoretical value. Even after 120 cycles, the value can still remain at 383.3 mAh g^{-1}. The capacity retention rate (C_{120}/C_{max}) is 62.9%. This may be due to its highest carbon amount and the largest BET surface area, which improve the electrical conductivity and the contact area of the electrode and electrolyte, further leading to the increasing utilization of the active material Co. And the Co@C-1 electrode displays the best cycle stabilities, which may be due to the ordered array of Co@C nanoparticles in nanorods that facilitated the electron transfer, leading to the enhanced electrochemical properties.[19,37] High rate performance is one of the most important factors evaluating a practical battery. The rate capability of the Co@C-1 electrode was measured at various discharging currents to examine the kinetic properties. As shown in Figure 6b, the discharge capacities of the Co@C-1 composite electrode are 610, 590, 570 and 470 mAh g^{-1}, respectively. The results indicate that the Co@C-1 composites could significantly possess high specific surface area and large channels among the nanostructures, provide more reaction sites for facile charge transfer and electrolyte penetration to enhance the electrochemical properties of the Co@C-1 composite electrode.

Figure 7a depicts the charge−discharge curves of the Co@C-1 electrode at the 1st, 2nd, 3rd, 10th and 30th cycles. As we can see from Figure 7a, the discharge capacity is 609 mAh g^{-1} at the 1st cycle and decreases to 472 mAh g^{-1} at the 30th cycle. Two potential plateaus have appeared in all the charge curves as well as one potential plateau of the discharge curves for each cycle. The first plateau of the charge process is at around −0.88 V, and the other one located at −1.02 V can be ascribed to the water electrolysis. The only plateau of discharge curves for each cycle centers at about −0.78 V. These results are accordant with the potential plateaus of the Co-based materials when used as the anode for the rechargeable Ni/Co batteries.[3,13,14,16,21,23,38] Figure 7b illustrates the CV curves of the Co@C-1 electrode in the first three cycles. For the Co@C-1 electrode, a cathodic peak appears at −0.98 V, and also an anodic current peak at near −0.72 V can be found in all the three CV cycles, corresponding to the reduction−oxidation reaction during charge/discharge procedure. Thus, the curve shape, the anodic and cathodic peak positions of the Co@C-1 electrode are highly accordant with the previous reported Co-based electrode material, demonstrating the same reduction−oxidation reaction.[3,38] In addition, the integral area of the CV curves gradually decreases, suggesting that the discharge capacity of the first three cycles gradually reduces, which further confirms the cycle performances results of the Co@C-1 electrode.

To further investigate the electrochemical reaction mechanisms of the Co@C-1 electrode during the charge and discharge processes, an XRD measurement was performed to characterize the composition of the Co@C-1 electrode at different charged/discharged states (Figure 8). The electrodes for XRD measurements are prepared by using acetylene black as a conductive agent instead of the carbonyl Ni, which is due to the strong intensity of the carbonyl Ni diffraction peaks. There is little cobalt hydroxide and metallic Co after the first fully charged process. And also, little amounts of Co and cobalt hydroxide appear at the first fully discharged state. After the second fully charged procedure, the cobalt hydroxide phase still exists as well as the metallic Co, suggesting a partially irreversible conversion of the metallic Co and cobalt hydroxide during the charge/discharge procedure. In addition, with the cycling, the diffraction intensity of cobalt hydroxide at the fully discharged state gradually increases. These indicate that the reduction−oxidation of the electrode irreversibility increases.

dx.doi.org/10.1021/am4048392 | ACS Appl. Mater. Interfaces 2014, 6, 3863−3869

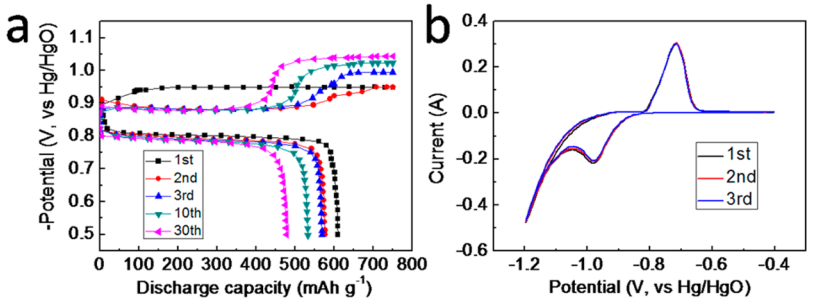

Figure 7. Charge−discharge curves (a) and CV curves (b) of the Co@C-1 electrode.

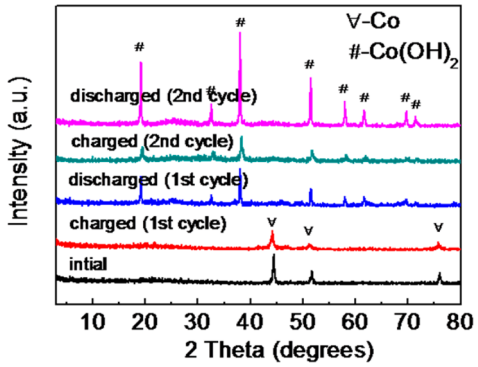

Figure 8. XRD patterns of the Co@C-1 electrode at charged or discharged states after first and second cycles.

On the basis of the above discussions, the reaction mechanism of the Co@C composite electrode during charge and discharge process can be ascribed to the redox reaction of Co and cobalt hydroxide.[15,19,21,39,40] In other words, during the discharge process, metallic Co is oxidated to cobalt hydroxide, and cobalt hydroxide is reduced to metallic Co under the charge procedure. This can be expressed in the following equation:

$$Co + 2OH^- \underset{\text{charge}}{\overset{\text{discharge}}{\rightleftharpoons}} Co(OH)_2 + 2e$$

There are several factors contributing to the Co@C composite having a high discharging capacity, excellent cycle performance and high rate capacity. First, the subsequent in situ process is beneficial to the formation of the Co@C hybrid material with high interfacial interaction between the C and Co nanoparticles. Second, the unity of the Co nanoparticles and high conductivity carbon supplies electron superhighways, which permit rapid and efficient charge transportation and result in the overall electronic conductivity increase. Third, the 1D porous nanostructure could reduce the transport path and offer a robust retention of electrolyte ions to meet the demands of fast charge and discharge reactions. And the large specific surface area could guarantee more effective contact between the electrolyte ions and the active materials, thus raising the electrochemical performance.

4. CONCLUSION

In summary, 1D porous Co@C nanorods have been successfully synthesized by pyrolysis of Co-based precursor (Co−NTA) nanorods. The Co@C nanorods show enhanced electrochemical performance used as an electrode material for alkaline secondary battery. The obtained porous Co@C electrode delivers a high discharge capacity of 609 mAh g^{-1} at 500 mA g^{-1}, desirable rate capacity (470 mAh g^{-1} at 1000 mA g^{-1}) and excellent stability (retains about 383.3 mAh g^{-1} after 120 cycles). The porous structure and large specific surface area have a significant effect on the electrochemical activity of Co@C. In addition, the dominate reduction−oxidation reaction of Co@C composite electrode is the conversion of Co and Cobalt hydroxide during the charge/discharge process.

■ ASSOCIATED CONTENT

Ⓢ Supporting Information

XRD pattern and Raman spectrum of the Co@C-1 composite, SEM images of the precursors H2, H3, Co@C-2 and Co@C-3, Nitrogen adsorption and desorption isotherms of the Co@C-2 and Co@C-3. This material is available free of charge via the Internet at http://pubs.acs.org.

■ AUTHOR INFORMATION

Corresponding Author

*Y. Wang. Tel/fax: +86-022-23503639. E-mail: wangyj@nankai.edu.cn.

Notes

The authors declare no competing financial interest.

■ ACKNOWLEDGMENTS

This work obtained financial supports from NSFC (21231005, 51071087), 973 (2011CB935900, 2010CB631303), 111 Project (B12015), Tianjin Sci & Tech Project (10SY-SYJC27600), Nature Science Foundation of Tianjin (11JCYBJC07700), and Research Fund for the Doctoral Program of Higher Education of China (20120031110001).

■ REFERENCES

(1) Sun, Y.; Xia, Y. Shape-Controlled Synthesis of Gold and Silver Nanoparticles. *Science* **2002**, *298*, 2176−2179.

(2) Burda, C.; Chen, X.; Narayanan, R.; El-Sayed, M. A. Chemistry and Properties of Nanocrystals of Different Shapes. *Chem. Rev.* **2005**, *105*, 1025−1102.

(3) Wang, Q. H.; Jiao, L. F.; Du, H. M.; Huan, Q. N.; Peng, W. X.; Song, D. W.; Wang, Y. J.; Yuan, H. T. Chainlike Structures Assembled by Co Hierarchitectures: Synthesis and Electrochemical Properties as Negative Materials for Alkaline Secondary Batteries. *J. Mater. Chem.* **2011**, *21*, 14159−14162.

(4) Tenne, R. Advances in the Synthesis of Inorganic Nanotubes and Fullerene-Like Nanoparticles. *Angew. Chem., Int. Ed.* **2003**, *42*, 5124−5132.

(5) Li, B. X.; Rong, G. X.; Xie, Y.; Huang, L. F.; Feng, C. Q. Low-Temperature Synthesis of α-MnO_2 Hollow Urchins and Their Application in Rechargeable Li^+ Batteries. *Inorg. Chem.* **2006**, *45*, 6404−6410.

(6) Hu, Z. A.; Xie, Y. L.; Wang, Y. X.; Xie, L. J.; Fu, G. R.; Jin, X. Q.; Zhang, Z. Y.; Yang, Y. Y.; Wu, H. Y. Synthesis of α-Cobalt Hydroxides

with Different Intercalated Anions and Effects of Intercalated Anions on Their Morphology, Basal Plane Spacing, and Capacitive Property. *J. Phys. Chem. C* **2009**, *113*, 12502−12508.
(7) Zhao, X. Y.; Ma, L. Q.; Shen, X. D. Co-Based Anode Materials for Alkaline Rechargeable Ni/Co Batteries: A Review. *J. Mater. Chem.* **2012**, *22*, 277−285.
(8) Kim, J. G.; Nam, S. H.; Lee, S. H.; Choi, S. M.; Kim, W. B. SnO_2 Nanorod-Planted Graphite: An Effective Nanostructure Configuration for Reversible Lithium Ion Storage. *ACS Appl. Mater. Interfaces* **2011**, *3*, 828−835.
(9) Cui, H. J.; Shi, J. W.; Yuan, B. L.; Fu, M. L. Synthesis of Porous Magnetic Ferrite Nanowires Containing Mn and Their Application in Water Treatment. *J. Mater. Chem. A* **2013**, *1*, 5902−5907.
(10) Chockla, A. M.; Klavetter, K. C.; Mullins, C. B.; Korgel, B. A. Solution-Grown Germanium Nanowire Anodes for Lithium-Ion Batteries. *ACS Appl. Mater. Interfaces* **2012**, *4*, 4658−4664.
(11) Cherian, C. T.; Sundaramurthy, J.; Reddy, M. V.; Suresh Kumar, P.; Mani, K.; Pliszka, D.; Sow, C. H.; Ramakrishna, S.; Chowdari, B. V. R. Morphologically Robust $NiFe_2O_4$ Nanofibers as High Capacity Li-Ion Battery Anode Material. *ACS Appl. Mater. Interfaces* **2013**, *5*, 9957−9963.
(12) Hu, C. C.; Chang, K. H.; Lin, M. C.; Wu, Y. T. Design and Tailoring of the Nanotubular Arrayed Architecture of Hydrous RuO_2 for Next Generation Supercapacitors. *Nano Lett.* **2006**, *6*, 2690−2695.
(13) Gao, X. P.; Yao, S. M.; Yan, T. Y.; Zhou, Z. Alkaline Rechargeable Ni/Co Batteries: Cobalt Hydroxides as Negative Electrode Materials. *Energy Environ. Sci.* **2009**, *2*, 502−505.
(14) Du, H. M.; Jiao, L. F.; Wang, Q. H.; Huan, Q. N.; Guo, L. J.; Si, Y. C.; Wang, Y. J.; Yuan, H. T. Morphology Control of $CoCO_3$ Crystals and Their Conversion to Mesoporous Co_3O_4 for Alkaline Rechargeable Batteries Application. *CrystEngComm* **2013**, *15*, 6101−6109.
(15) Song, D. W.; Xu, Y. N.; An, C. H.; Wang, Q. H.; Wang, Y. P.; Li, L.; Jiao, L. F.; Yuan, H. T. Recovered $LiCoO_2$ as Anode Materials for Ni/Co Power Batteries. *Phys. Chem. Chem. Phys.* **2012**, *14*, 71−75.
(16) Li, L.; Xu, Y. N.; An, C. H.; Wang, Y. J.; Jiao, L. F.; Yuan, H. T. Enhanced Electrochemical Properties of Co/CMK-3 Composite as Negative Material for Alkaline Secondary Battery. *J. Power Sources* **2013**, *238*, 117−122.
(17) Aricò, A. S.; Bruce, P.; Scrosati, B.; Tarascon, J. M.; Van Schalkwijk, W. Nanostructured Materials for Advanced Energy Conversion and Storage Devices. *Nat. Mater.* **2005**, *4*, 366−377.
(18) Guo, Y. G.; Hu, J. S.; Wan, L. J. Nanostructured Materials for Electrochemical Energy Conversion and Storage Devices. *Adv. Mater.* **2008**, *20*, 2878−2887.
(19) Lu, D. S.; Li, W. S.; Xiao, F. M.; Tang, R. H. Drastically Enhanced Cycle Life of Co-B alloy Electrode by 8-Hydroxyquinoline at Elevated Temperature. *Electrochem. Commun.* **2010**, *12*, 362−366.
(20) Wang, Y. D.; Ai, X. P.; Yang, H. X. Electrochemical Hydrogen Storage Behaviors of Ultrafine Amorphous Co−B Alloy Particles. *Chem. Mater.* **2004**, *16*, 5194−5197.
(21) Song, D. W.; Wang, Y. J.; Wang, Q. H.; Wang, Y. P.; Jiao, L. F.; Yuan, H. T. Effect and Function Mechanism of Amorphous Sulfur on the Electrochemical Properties of Cobalt Hydroxide Electrode. *J. Power Sources* **2010**, *195*, 7115−7119.
(22) Li, L.; Wang, Y. P.; Wang, Y. J.; Han, Y.; Qiu, F. Y.; Liu, G.; Yan, C.; Song, D. W.; Jiao, L. F.; Yuan, H. T. Mesoporous Nano-Co_3O_4: A Potential Negative Electrode Material for Alkaline Secondary Battery. *J. Power Sources* **2011**, *196*, 10758−10761.
(23) Han, Y.; Wang, Y. J.; Wang, Y. P.; Jiao, L. F.; Yuan, H. T.; Liu, S. X. Hydrothermal Synthesis and Electrochemical Properties of Cobalt−carbon Nanotubes Nanocomposite. *Electrochim. Acta* **2011**, *56*, 3258−3263.
(24) Du, H. M.; Jiao, L. F.; Wang, Q. H.; Peng, W. X.; Song, D. W.; Wang, Y. J.; Yuan, H. T. Structure and Electrochemical Properties of Ball-Milled Co-Carbon Nanotube Composites as Negative Electrode Material of Alkaline Rechargeable Batteries. *J. Power Sources* **2011**, *196*, 5751−5755.
(25) Lee, H.; Yoon, S. W.; Kim, E. J.; Park, J. In-Situ Growth of Copper Sulfide Nanocrystals on Multiwalled Carbon Nanotubes and Their Application as Novel Solar Cell and Amperometric Glucose Sensor Materials. *Nano Lett.* **2007**, *7*, 778−784.
(26) Ji, K. H.; Jang, D. M.; Cho, Y. J.; Myung, Y.; Kim, H. S.; Kim, Y.; Park, J. Comparative Photocatalytic Ability of Nanocrystal-Carbon Nanotube and -TiO_2 Nanocrystal Hybrid Nanostructures. *J. Phys. Chem. C* **2009**, *113*, 19966−19972.
(27) Tsuboi, M.; Onishi, K.; Nakagawa, I.; Shimanouchi, T.; Mizushima, S. A Multi-Model Fusion Strategy for Multivariate Calibration Using Near and Mid-Infrared Spectra of Samples from Brewing Industy. *Spectrochim. Acta* **1958**, *12*, 253.
(28) Liu, S.; Li, L. M.; Hao, Q. Y.; Yin, X. M.; Zhang, M.; Li, Q. H.; Chen, L. B.; Wang, T. H. A Novel Non-Enzymatic Hydrogen Peroxide Sensor Based on Mn-Nitrilotriacetate Acid (Mn-NTA) Nanowires. *Talanta* **2010**, *81*, 727−731.
(29) Li, C. C.; Mei, L.; Chen, L. B.; Li, Q. h.; Wang, T. H. Synthesis of Highly Aligned and Ultralong Coordination Polymer Nanowires and Their Calcination to Porous Manganese Oxide Nanostructures. *J. Mater. Chem.* **2012**, *22*, 4982.
(30) Wang, G. X.; Gou, X. L.; Horvat, J.; Park, J. Facile Synthesis and Characterization of Iron Oxide Semiconductor Nanowires for Gas Sensing Application. *J. Phys. Chem. C* **2008**, *112*, 15220−15225.
(31) Liu, H.; Wexler, D.; Wang, G. X. One-Pot Facile Synthesis of Iron Oxide Nanowires as High Capacity Anode Materials for Lithium Ion Batteries. *J. Alloys Compd.* **2009**, *487*, L24−L27.
(32) Li, C. C.; Yin, X. M.; Chen, L. B.; Li, Q. H.; Wang, T. H. Synthesis of Cobalt Ion-Based Coordination Polymer Nanowires and Their Conversion into Porous Co_3O_4 Nanowires with Good Lithium Storage Properties. *Chem.—Eur. J.* **2010**, *16*, 5215−5221.
(33) Cuesta, A.; Dhamelincourt, P.; Laureyns, J.; Martínez-Alonso, A.; Tascón, J. M. D. Raman Microprobe Studies on Carbon Materials. *Carbon* **1994**, *32*, 1523−1532.
(34) Stankovich, S.; Dikin, D. A.; Piner, R. D.; Kohlhaas, K. A.; Kleinhammes, A.; Jia, Y. Y.; Wu, Y.; Nguyen, S. T.; Ruoff, R. S. Synthesis of Graphene-Based Nanosheets via Chemical Reduction of Exfoliated Graphite Oxide. *Carbon* **2007**, *45*, 1558−1565.
(35) He, Y.; Huang, L.; Li, X.; Xiao, Y.; Xu, G. L.; Li, J. T.; Sun, S. G. Facile Synthesis of Hollow Cu_2Sb@C Core-Shell Nanoparticles as a Superior Anode Material for Lithium Ion Batteries. *J. Mater. Chem.* **2011**, *21*, 18517−18519.
(36) Sun, S. G. Facile Synthesis of Porous MnO/C Nanotubes as a High Capacity Anode Material of Lithium Ion Batteries. *Chem. Commun.* **2012**, *42*, 8502−8504.
(37) Saravanan, K.; Ananthanarayanan, K.; Balaya, P. Mesoporous TiO_2 with High Packing Density for Superior Lithium Storage. *Energy Environ. Sci.* **2010**, *3*, 939−948.
(38) Wang, Y. P.; Li, L.; Wang, Y. J.; Song, D. W.; Liu, G.; Han, Y.; Jiao, L. F.; Yuan, H. T. Crystalline CoB: Solid State Reaction Synthesis and Electrochemical Properties. *J. Power Sources* **2011**, *196*, 5731−5736.
(39) Elumalai, P.; Vasan, H. N.; Munichandraiah, N. Electrochemical Studies of Cobalt Hydroxide — An Additive for Nickel Electrodes. *J. Power Sources* **2001**, *93*, 201−208.
(40) Wang, Q. H.; Jiao, L. F.; Du, H. M.; Peng, W. X.; Liu, S. C.; Wang, Y. J.; Yuan, H. T. Electrochemical Hydrogen Storage Property of Co−S Alloy Prepared by Ball-Milling Method. *Int. J. Hydrogen Energy* **2010**, *35*, 8357−8362.